ISEIS

Journal of Environmental Informatics 44(2) 112-125 (2024)

Journal of Environmental Informatics

www.iseis.org/jei

# Estimation of Water Surface Reflectance and Total Suspended Solid Using MODIS Images for a Reservoir in the Brazilian Semiarid Region

V. N. L. Rocha[1], C. A. G. Santos[1] *, and R. M. Silva[2]

[1] *Department of Civil and Environmental Engineering, Federal University of Paraíba, 58051-900 João Pessoa, Brazil*
[2] *Department of Geosciences, Federal University of Paraíba, 58051-900 João Pessoa, Brazil*

Received 04 August 2022; revised 20 September 2022; accepted 07 September 2023; published online 05 September 2024

**ABSTRACT.** Reservoirs are essential sources to ensure water supply, especially in regions with a semiarid climate, prone to prolonged drought periods and water scarcity. An exemplary case is the semiarid region of Paraíba State, Brazil. Monitoring of water surface reflectance (WSR) and total suspended solids (TSS) is indispensable to address issues such as erosion, sediment transport, deposition, reservoir siltation, water pollution, and associated human health risks, ultimately aiding in water resources management. This study introduced a novel approach to estimating the spatiotemporal dynamics of WSR and TSS, utilizing automated methods and MODIS images over 17 years (2000 ~ 2016) for the Epitácio Pessoa Reservoir. Three models, (a) model 1 (M1), (b) model 2 (M2), and (c) model 3 (M3), were employed to estimate WSR and TSS, chosen for their replicability, mathematical simplicity, and ecosystem similarity. A total of 775 images from the Moderate Resolution Imaging Spectroradiometer (MODIS) onboard the Terra satellite, along with observed data, were used for the estimation. Model M3 yielded the best performance for estimating TSS, with values ranging from 270 ~ 961 mg/L ($r = 0.57$). Furthermore, a strong correlation ($r > 0.93$) was observed between the mean reflectance values for pixels sampled using two distinct extraction procedures (longitudinal profile and specific sampling points). This strong correlation underscores the potential utility of MODIS images for effective monitoring of WSR and TSS in comparatively smaller bodies of water in the Brazilian semiarid region. Importantly, this study represents one of the first applications for estimating WSR and TSS for a reservoir situated in a semiarid climate region. The estimates of WSR and TSS could hold significant implications for environmental monitoring and water management of such reservoirs. In conclusion, automated estimation of WSR and TSS could serve as a valuable tool for decision-makers in predicting silting, sediment yield, and reservoir water quality.

*Keywords:* remote sensing, MOD09Q1, Epitácio Pessoa Reservoir, total suspended solids, water scarcity, semiarid climate

## 1. Introduction

Reservoirs in the Brazilian semiarid region are critical for water supply due to the persistent water scarcity resulting from frequent drought periods (Zhang et al., 2016; Viana et al., 2021; Lima Neto et al., 2022). Factors such as low average rainfall, extended drought periods (Azevêdo et al., 2017; Yunus et al., 2021), high evapotranspiration rates, and extreme rainfall events that transport large volumes of sediment (Brasil Neto et al., 2022) contribute to high stress on the volume of water in these reservoirs. The reservoirs serve as the primary source of water storage for many urban areas and a significant portion of agricultural activities in the Brazilian semiarid region (Silva et al., 2020; Assis et al., 2021; Sousa et al., 2021) and are susceptible to climate variability and intense modification of land use and cover (Fonseca et al., 2022; Luo et al., 2022). These modifications have direct impacts on the water quality and transported sediment. Estimating turbidity and total suspended solids (TSS) in inland waters can help monitor sediment discharge and, more generally, the sediment budget within catchments and its seasonal variability and evolution over time. Therefore, knowing the behavior of the seasonal variability of the TSS is essential for better management of water resources and planning of water use to meet the demands (Condé et al., 2019; Jiang et al., 2021). The assessment and monitoring of TSS is crucial information for effective reservoir management. Extreme rainfall events and inadequate land-use management influence the sediment yield and the silting process in the reservoirs in a semiarid environment. The management of TSS and associated contaminants in the rivers requires knowledge of the sediment sources (Isidro et al., 2018).

However, conventional monitoring techniques for hydrologic studies, despite their importance, can be expensive, time-consuming, and offer limited spatiotemporal frequency. These limitations highlight the need for alternative methods, such as the estimation of water surface reflectance (WSR) and total suspended solid using MODIS images, which offer a more efficient and cost-effective means of collecting data for monitoring water quality in large bodies of water over time (Santos et al., 2021). Thus, the use of remote sensing applied to water resources stands

* Corresponding author. Tel.: +55-833-217-7684; fax: +55-833-216-7179.
*E-mail address*: celso@ct.ufpb.br (C. A. G. Santos).

ISSN: 1726-2135 print/1684-8799 online
© 2024 ISEIS All rights reserved. doi:10.3808/jei.202400527

out. The use of remote sensing demonstrates the potential for generating data with greater temporal representation in water quality monitoring and sediment dynamics estimation (Pinto et al., 2014; Bernardo et al., 2016). Several empirical methods have been developed to retrieve TSS using remote sensing (Han et al., 2006; Sahoo et al., 2022). For instance, Tassan (1993) and Zhang et al. (2010) used an empirical relationship to map the TSS concentration using Landsat TM data. Brown et al. (2008) and Miller and McKee (2004) used MODIS products to monitor TSS. Mao et al. (2012) showed the potential of the TSS model enhanced by a combination of semi-analytical and empirical approaches and introduced a new model by a combination of an empirical and semi-analytical algorithm to estimate the TSS concentration. Nechad et al. (2010) developed a multisensor model to recover the TSS concentration in turbid water using a hyperspectral calibration to identify the best spectral range from reflectance data collected by MERIS, MODIS, and SeaWiFS sensors. Pinto et al. (2014) monitored the inflow of sediments using MODIS images, the MOD3R algorithm, and observed data. Manoppo and Budhiman (2017) applied the Landsat OLI/TIRS to estimate TSS concentrations in coastal waters. All these works presented empirical methods and have been applied to various optical satellite data. To this end, the reflectance at different bands is determined, and then statistical relationships between observed and remote sensing data are generated. Thus, the relationship between the measured remote sensing reflectance data in various spectrum portions is a common empirical method to estimate TSS and WSR.

Previous studies have provided valuable insights into various aspects of water quality monitoring and sediment dynamics estimation using remote sensing techniques (Pinto et al., 2014; Bernardo et al., 2016). However, there is a gap in the research as most studies have focused on large water bodies and made use of single-model applications, leaving a gap in understanding the efficacy of these techniques when applied to smaller water bodies in semiarid regions. Moreover, the focus of most previous research has been on monitoring rather than estimation, with limited attention to the importance of accurately estimating WSR and TSS in the context of water management (Condé et al., 2019; Jiang et al., 2021).

Recently, several studies have been conducted to estimate chlorophyll using satellite images (Chen et al., 2015; Watanabe et al., 2015; Kim et al., 2017), turbidity (Pahlevan and Schott, 2012; Robert et al., 2016), cyanobacteria and phytoplankton pigments (Becker et al., 2009). In recent decades, there has been a growing use in the application of MODIS images to estimate suspended sediments in oceanic waters, rivers, large lakes, and estuaries (Dorji et al., 2016; Kumar et al., 2016; Isidro et al., 2018), and many studies have demonstrated a strong correlation between WSR and TSS. However, the nature of the relationship between TSS and reflectance varies from place to place due to the varying nature of the optical properties of different bodies of water and the procedure for collecting field samples during different seasons (Kumar et al., 2016). Currently, there is a need for more studies on TSS and WSR for the Brazilian semiarid region. For instance, Pereira et al. (2019) evaluated the concentration of WSR and TSS using only one model to estimate TSS in an intermittent river, typical of the Brazilian semiarid region using high to medium spatial resolution images. The results showed that the hydrological characteristics of intermittent semiarid rivers generate difficulties in monitoring TSS using optical satellite remote sensing.

Three models are considered for this study: model 1 (M1) (Miller and McKee, 2004), model 2 (M2) (Villar et al., 2013), and model 3 (M3) (Robert et al., 2017). They were chosen based on their replicability, mathematical simplicity, and applicability to environments similar to those in the semiarid regions, especially for continental waters. Each model uses the same input data, MOD09Q1 V006, and operates within a minimum TSS amplitude of 60 mg/L. While these models have been tested in humid environments by their authors, their effectiveness has yet to be confirmed under the unique conditions of the semiarid region of northeastern Brazil, characterized by extreme rainfall and drought events.

This research addresses the existing gap in the literature by applying these three models to estimate the spatiotemporal dynamics of WSR and TSS in a semiarid region. The Epitácio Pessoa Reservoir serves as the case study for this research, with the models applied to MODIS images spanning from 2000 to 2016. The aim of this research extends beyond merely monitoring the reservoir; it seeks to accurately estimate WSR and TSS, with the goal of providing data that can inform decision-making in water resource management in similar contexts. By enhancing the understanding of reservoir dynamics through the estimation of the spatiotemporal dynamics of WSR and TSS, this study intends to contribute to more informed decision-making and effective planning for future water use and reservoir management in the Brazilian semiarid region.

## 2. Materials and Methods

### 2.1. Study Area

The Epitácio Pessoa Reservoir (Figure 1), built in 1957, has a maximum design volume capacity of 411,686,287 $m^3$. It is located between the coordinates 07°25′10″ ~ 07°32′15″ S, and 36°07′20″ ~ 36°20′05″ W. It is important to note that reservoir construction is a public policy in Brazil, implemented to mitigate the effects of drought (Silva et al., 2021). This policy provides significant relief to the vulnerable population in the Brazilian semiarid region (Dantas et al., 2020). The reservoir is a primary water source for 19 cities in the Paraíba State, the most important of which is Campina Grande (AESA, 2016). Situated in the Brazilian semiarid region, specifically in the central portion of Paraíba State on the Borborema Plateau, the Epitácio Pessoa Reservoir experiences a warm semiarid climate (BSh), according to the Köppen-Geiger classification, with a dry season between June and December (Silva et al., 2021). The mean annual rainfall ranges from 500 to 750 mm, typically occurring between January and May (Medeiros et al., 2019). The Epitácio Pessoa Reservoir is among the main reservoirs within the semiarid area of Paraíba State and serves as the primary water source for millions of users in the region. With a significant socioeconomic and environmental impact, the reservoir supplies water to about

1 million inhabitants. Therefore, understanding the siltation level and water quality in this reservoir is crucial for regional water management and the security of the population that depends on this reservoir.

### 2.2. Images and Data Processing

This study involved an automated selection, filtering, cloud cleaning, and estimation of WSR and TSS, using models from the existing literature to estimate TSS values in a reservoir located in a semiarid climate. The MODIS surface reflectance product MOD09Q1 V006, which provides calibrated reflectance for bands at 250 m resolution, was employed. The MOD09Q1 V006 includes four different types of products: (a) $R_{RED}$ reflectance layer in the red spectrum (620 ~ 670 nm), (b) $R_{NIR}$ reflectance layer in the near-infrared spectrum (841 ~ 876 nm), (c) state flag quality layer, and (d) quality control layer. MODIS surface reflectance 8-day composite data from March 2000 to December 2016 were downloaded from the USGS/NASA LP DAAC digital collection. A total of 775 images, averaging 46 images per year, were analyzed. Each image is a pixel-by-pixel composite product that has undergone geometric correction. The best pixels are selected within an 8-day time interval that demonstrated the best quality with respect to the absence of noise, such as clouds and shadows (Vermote et al., 1997). These images have atmospheric effect corrections and are georeferenced in sinusoidal projection (Vermote, 2015). As Robert et al. (2016) indicated, composite images were chosen for longterm monitoring because the 8-day composite aligns with the 5- and 7-day field measurement sampling frequency. Moreover, these images moderate the bidirectional reflectance effects and atmospheric artifacts.

Data processing was executed as depicted in Figure S1, starting with preprocessing. This stage involved converting the HDF extension image database (*.hdf) to the GeoTIFF image format (*.tif) and transitioning from the sinusoidal projection (SIN) to Universal Transverse Mercator (UTM) plane coordinates. Subsequently, the spatial clipping of the tiles (h14v09) was performed, and the output was converted to ASCII extension.

Before extracting the reflectance values of $R_{RED}$ and $R_{NIR}$, all 775 scenes were filtered by comparing their reflectance bands with the state flag layer. This procedure followed the steps illustrated in Figure S1. A Matlab script was developed to filter out cloud-free pixels (*Cloud-Free* – F-1). This script effectively compared each pixel of the $R_{RED}$ and $R_{NIR}$ bands to the corresponding state flag pixel across all scenes, thereby only extracting cloud-free pixels. The most stringent condition was applied by evaluating the binary values of each pixel's 2nd and 3rd bit-strings; only pixels with a value of '00' (indicating clear conditions) were considered acceptable.

Following the filtering process, it was discovered that, due to the geometry and seasonality of the reservoir's water surface, some pixels seemed to reflect objects other than water or displayed spectral mixing. To identify and discard these instances, a second filtering step, referred to as F-2 (Figure S1), was implemented. This step involves the selection of the most frequently occurring pixels in the water surface throughout the analyzed time series, i.e., those that are water pixels with a higher homogeneity content. To identify these sampling points, it was necessary to procure complementary multispectral products from other satellites, including Landsat 5, 7, and 8, CBERS 2, and RapidEye 3A. These satellites offer more refined spatial resolutions (between 5 and 30 m), and their images were obtained from the INPE (http://www.dgi.inpe.br/CDSR/) and GeoCatalogo/MMA (http://geocatalogo.mma.gov.br/) platforms. This study also utilized the Shuttle Radar Topography Mission (SRTM) radar altimetry from the United States Geological Survey (https://earthexplorer.usgs.gov/) with a 90 m resolution, and field bathymetry (https://metadados.snirh.gov.br/) produced by the National Water and Sanitation Agency of Brazil (ANA, 2013). After georeferencing, the multispectral images facilitated (a) the vectorization of the reservoir surface area for each year (Figure 2a), (b) the definition of the reservoir's longitudenal/thalweg profile using the bathymetry (Figure 2b), and (c) the selection of the spatially distributed pixels throughout the reservoir surface area (Figure 2c). Using the vectorized mask of each year in the series (step F-2), it was possible to exclude the pixels not located within the reservoir surface area.

To determine the longitudinal profile, 57 continuous pixels along the thalweg, representing the line of lowest elevation within the channel, were selected (Figure 2b). After this, 46 pixels within the reservoir surface area were chosen as sampling points (Figure 2c). The selection was based on equidistant spatial distribution criteria, and such pixels should be as far away as possible from the reservoir surface area margins. This resulted in 103 reflectance time series (Figure 2). However, only the time series with at least 10% of cloud-free pixels were considered in this study, yielding 39 and 37 time series, respectively.

### 2.3. WSR and TSS Estimation Models

In this study, the estimation and comparison of WSR and TSS were performed using the models M1, M2, and M3. The M1 model has been applied in various humid environments (e.g., lakes, deltas, and meanders), showing a strong linear relationship between $R_{RED}$ reflectance and field data of TSS concentration ($R^2 = 0.89$; N = 52; MSE = 4.74; range = 0 ~ 60 mg/L) (Miller and McKee, 2004). This model has been replicated in other studies (Mishra, 2010; Chen et al., 2015; Kumar et al., 2016) with regional data calibration, delivering satisfactory results.

The M2 model, developed by Villar et al. (2013), is designed to estimate TSS values specifically for the Madeira River in the Amazon River basin. It utilizes the relationship between the reflectance pairs of the $R_{RED}$ and $R_{NIR}$ bands, showing a good correlation of 0.78 between the band balance and suspended sediment data, with the correlation between field reflectance and observed suspended sediment data being 0.95.

The M3 model was proposed for lakes in the Sahel, an African semiarid region. Unlike M1 and other straightforward models, the M3 model takes into account the $R_{NIR}$ band. A correlation of approximately 70% was found between orbital and field-observed TSS data. It is noteworthy, however, that both orbital data from MODIS (60 samples) and Landsat satellite (37 samples) were used in the modeling. Another important aspect is that the observed TSS values ranged from 106 to 4,178 mg/L, highlight-

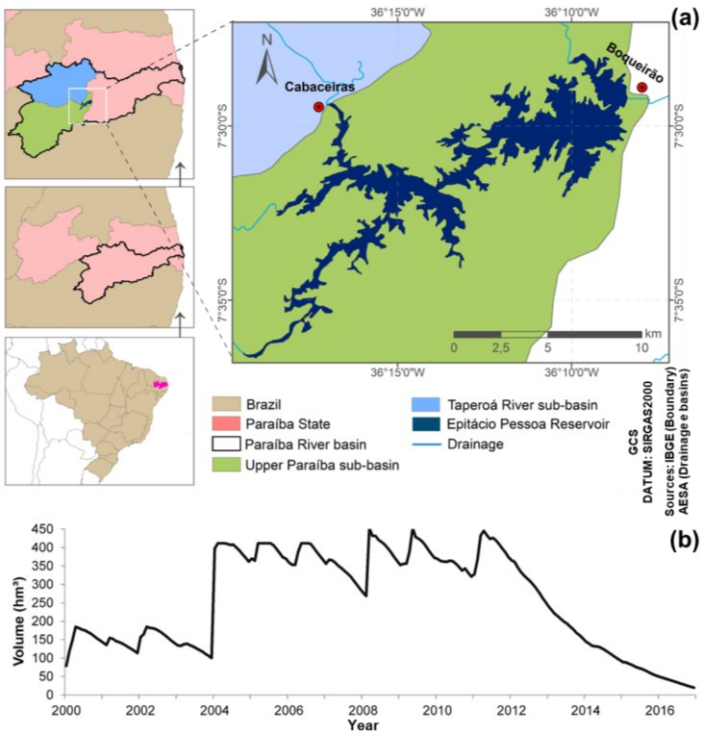


**Figure 1.** (a) Geographic location of the Epitácio Pessoa Reservoir in Paraíba State and Brazil, and (b) time series of the reservoir volume (2000 ~ 2016).

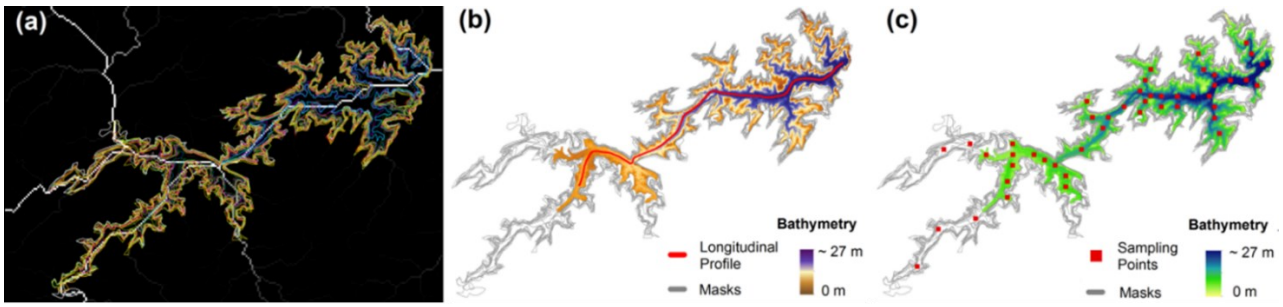


**Figure 2.** (a) Integration of vector data with the SRTM drainage network; (b) longitudinal profile (thalweg) of the Epitácio Pessoa Reservoir, depicted along with the bathymetry (shown in color); (c) selected sample pixels distributed throughout the reservoir's surface area, again accompanied by the bathymetry (shown in color).

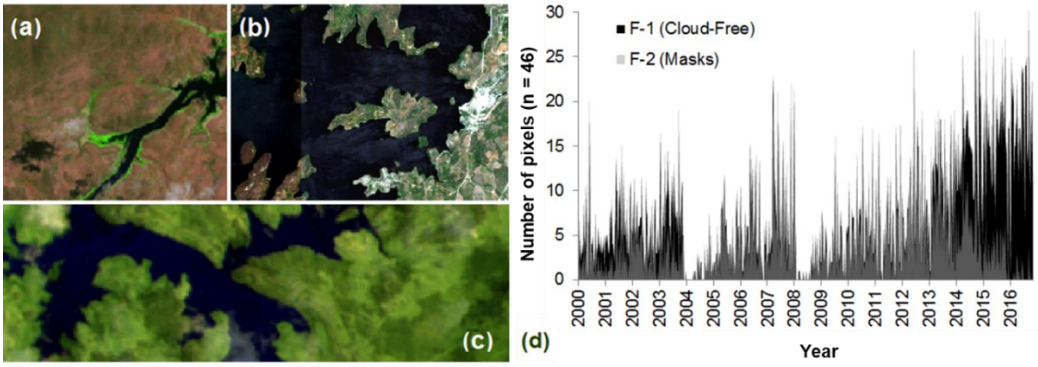


**Figure 3.** Examples of (a, b, c) interferences found during the extraction of WSR data in the reservoir and (d) quantity of pixels after removal with the two filters.

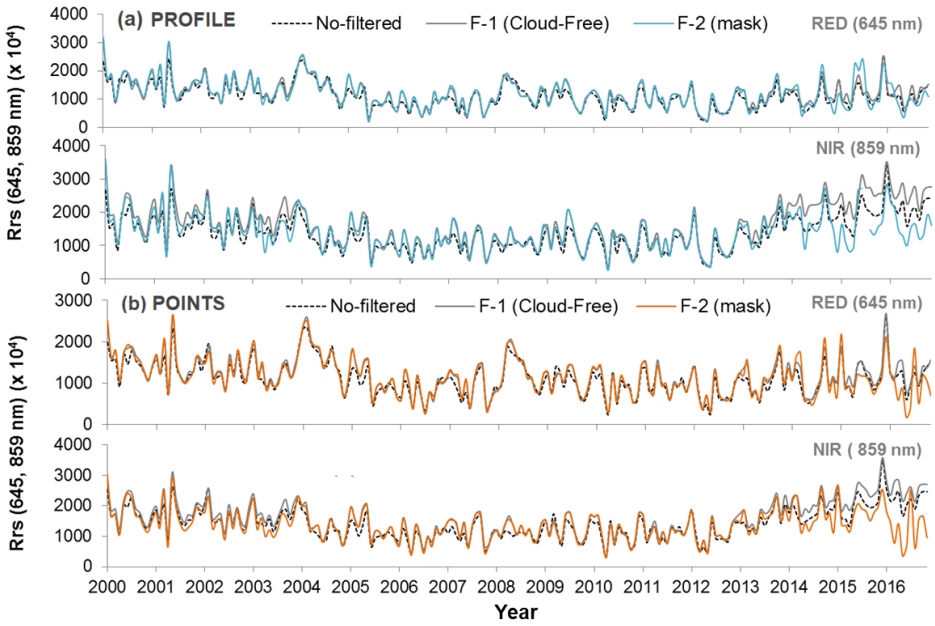


**Figure 4.** WSR time series (non-filtered and post-filtered 1 and 2) for $R_{RED}$ (645 nm) and $R_{NIR}$ (859 nm) bands, with monthly mean (a) longitudinal profiles (N = 39), and (b) sampling points (N = 37), from 2000 to 2016.

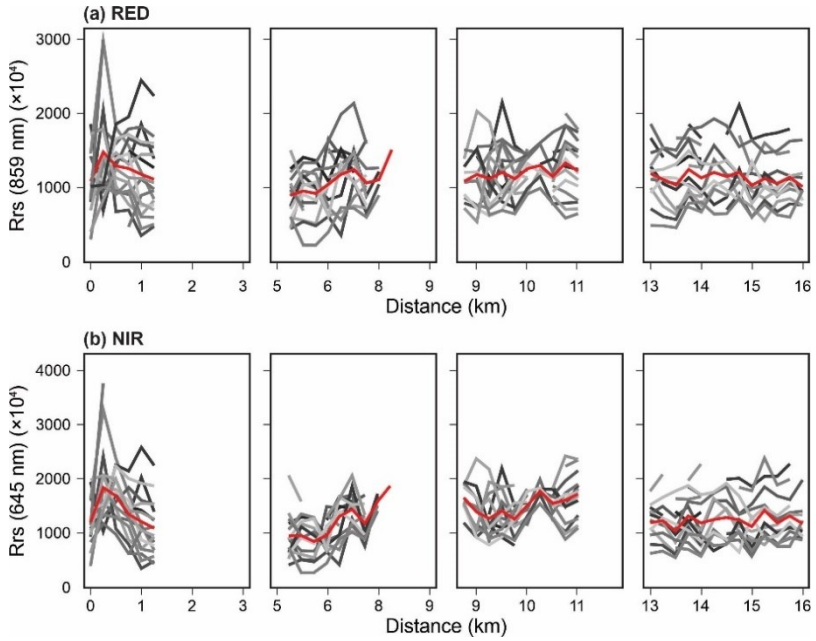


**Figure 5.** WSR values of the (a) $R_{RED}$ and (b) $R_{NIR}$ bands, including annual and global averages for the $R_{RED}$ band, across longitudinal profile pixels (N = 39) from 2000 to 2016.

ing the considerable TSS amplitude in arid environments.

## 3. Results

### 3.1. Uncertainties in WSR Data

Figure 3 presents the interferences observed during the extraction of WSR data in the reservoir and the temporal distribution of pixels number after removal using steps F-1 and F-2 (Figure S1). The results indicate that due to the geometrical characteristics of the reservoir surface area and the topographic nature of the region, some interferences in the pixel composition often occur during the initial process of determining the pixels from time series with spectral mixing. The sources of these uncertainties are visually represented in Figure 3. Figure 3a illustrates the presence of vegetation at the boundary or aquatic macrophytes. Figure 3b highlights the existence of surface is-

lands within the reservoir. Additionally, potential bottlenecks in the channel contribute to these uncertainties. Lastly, Figure 3c depicts the presence of clouds as another factor affecting the uncertainties.

It is worth noting that step F-2 enabled an evaluation of these uncertainties. The influence of annual mask vectorization on the relationship between the spectral bands [(Rrs 859 nm) / (Rrs 645 nm) > 1.5] is significant, as ratio values above 1.5 ($R_{NIR}$ / $R_{RED}$) indicate the presence of land and emerging vegetation in the water. Therefore, the number of pixels with ratio values ≤ 1.5 was analyzed (Figure 3d) using steps F-1 and F-2.

The results demonstrate significant pixel removal in certain years, particularly in the last years of the time series (2013 to 2016), which corresponds to a period of severe drought in the region (Dantas et al., 2020; Silva et al., 2020). Conversely, there is less intensity of removed values in other years, representing less than 8% of the total. Another noteworthy aspect is the intense interannual variability of the water mirror area in the study area. For instance, when comparing the minimum water mirror area in 2016 to the maximum area in 2005, there is an increase of 665%, a feature commonly found in reservoirs of semiarid regions. Thus, defining a fixed water surface in such areas presents a challenge.

### 3.2. Spatiotemporal Analysis of the WSR

Figure 4 illustrates the WSR time series (non-filtered, post-filtered using F-1 and F-2) for the $R_{RED}$ and $R_{NIR}$ bands from 2000 to 2016. In general, the $R_{RED}$ band dataset shows lower values compared to the $R_{NIR}$ band dataset. For the $R_{NIR}$ band dataset, the mean standard deviation of the reflectance ranged from 0.10 to 0.26, with an overall mean of 0.11. In contrast, for the $R_{NIR}$ band dataset, the mean standard deviation of the reflectance ranged from 0.30 to 0.32, with an overall mean of 0.13.

The results showed high reflectance values for water, ranging from 0 to 25% in the $R_{RED}$ band, which are consistent with values observed in reservoirs within the Brazilian semiarid region. Upon comparing raw values after cloud filtering (step F-1) and post heterogeneous pixels removal (step F-2), certain periods within the examined time frame exhibited under- and overestimated values of reflectance in raw data averages for both bands. Particularly in 2013, the $R_{NIR}$ band showed the highest sensitivity, with the final filtered values (using step F-2) being lower than both the raw values and the cloud-filtered values (using step F-1). From a spatial perspective, Figure 5 presents the average pixel values of the reservoir's longitudinal profile in both spectral bands, from the reservoir entrance to the dam wall (Figure 2b), spanning a length of 16 kilometers. However, the spatial analysis of the series for the longitudinal profile was not fruitful due to significant gaps in removed pixels.

The results reveal the first and largest gap as a 4 km stretch (from 1.2 to 5.2 km). This gap results from a high prevalence of clouds in the pixels of this range throughout the time series, leaving pixels without data after the F-1 filtering or with poor usability. Meanwhile, the two other data gaps (at 8 km and between 11 and 13 km), shown in Figure 5, were due to the F-2 filtering step, corroborating the challenges of obtaining continuous spatial data owing to the geometric characteristics of reservoirs in semiarid regions. Certain areas where pixels spatially coincide with water mirror contractions, given the 250 m spatial resolution, contain some pixels that exceed the area of the water mirror.

Figure 6 shows the average values of each series (pixel) from January to December for the longitudinal profile data (Figure 6a) and sampling points (Figure 6b). The results show that the $R_{NIR}$ band values exhibited more variation concerning the global mean values (represented by red and yellow lines) than the $R_{RED}$ band did. Global mean WSR values ranged from 0.09 to 0.18, corroborating other studies in semiarid regions, with peak values in February and minimum values in May, suggesting an influence of rainfall over the reservoir drainage areas.

Figure 7 shows the correlation between the annual and monthly averages of the two data/pixel sampling forms. The presented results show the similarity between the pattern of the independently extracted temporal (monthly and annual) averages data (longitudinal profile and sampling points) and a very strong correlation (> 0.93). As previously mentioned, in the temporal behavior, the data (inter- and intra-annual) showed signs of reflecting the rainfall behavior of their drainage basins. Thus, the results were compared with data from two rain gauges within the region (Figure 8).

According to AESA (2018) and Silva et al. (2021), the Epitácio Pessoa Reservoir basin is influenced by two climatic phenomena: A wet period in the first four months of the year (January ~ April) and recurring precipitation in June in parts of the region. The Monteiro rainfall station (MT, Figure 9a), located in the southwest portion of the basin, presents rainfall patterns as described in the first phenomenon, whereas the Campina Grande station (CG, Figure 9a), situated in the central-east of the basin (near the basin), indicates peak current precipitation in June.

The results (Figure 8a) indicate that the highest monthly reflectance averages (WSR) occur from January to March and in June for the $R_{NIR}$ band, with a slight reduction for the $R_{RED}$ band (exhibiting lower values in December). Consequently, it is evident that the reservoir responds to the rainfall patterns that occur in Paraíba State.

Another significant characteristic is the annual reflectance averages (Figure 8b). In most years, the WSR values of the $R_{NIR}$ band are higher than those of the $R_{RED}$ band, except in 2004 and 2008, with a more pronounced disparity in 2004. This is likely due is the sudden changes in reservoir volume (Figure 1b), which from 2003 to 2004 increased by over 300 $hm^3$, and from 2007 to 2008 saw an increase of over 150 $hm^3$. Both periods (2004 and 2008) were marked by overflow and drop in water levels, probably as a result of droughts. Changes in the reservoir volume over a short period, coupled with the prevalence of droughts, lead to a change in the type of sediment carried, thereby impacting the spectral response (WSR).

Therefore, in this regard, further investigation in the area is recommended. This could include an analysis of sediment fractions (volatile, fixed, dissolved, particle size, among others) to evaluate changes in the sediment composition of water that,

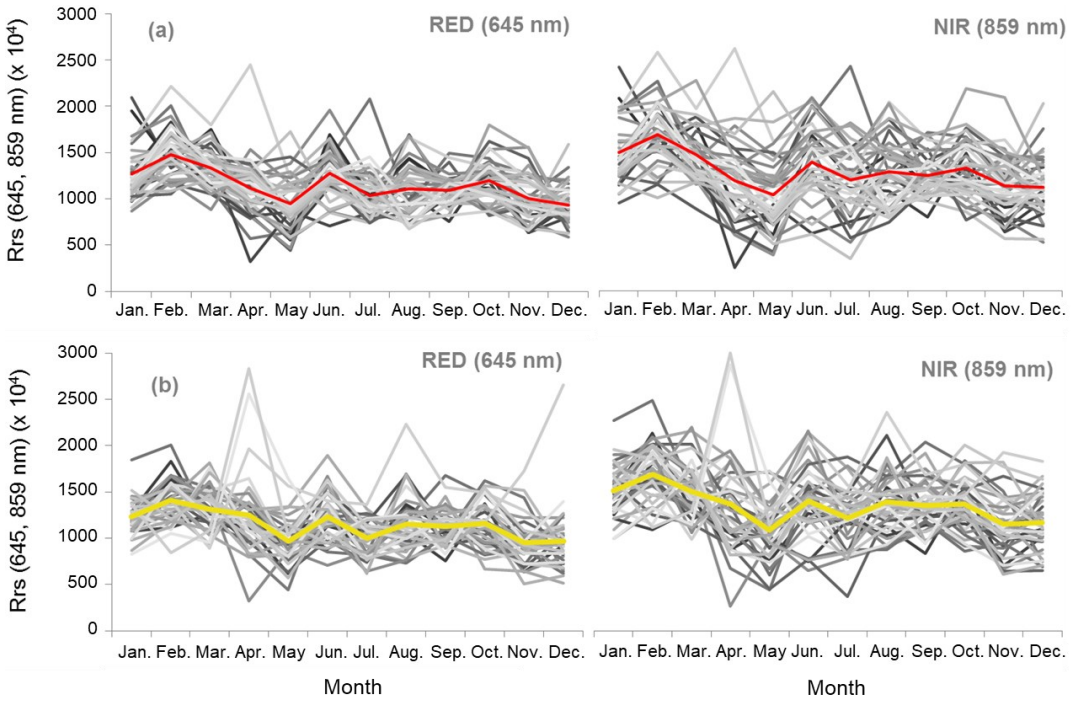


**Figure 6.** Filtered WSR time series for $R_{RED}$ (645 nm) and $R_{NIR}$ (859 nm) bands, displaying monthly pixel averages for (a) longitudinal (N = 39) and global (red) profiles, (b) sample points (N = 37), and overall (yellow), spanning 2000 to 2016.

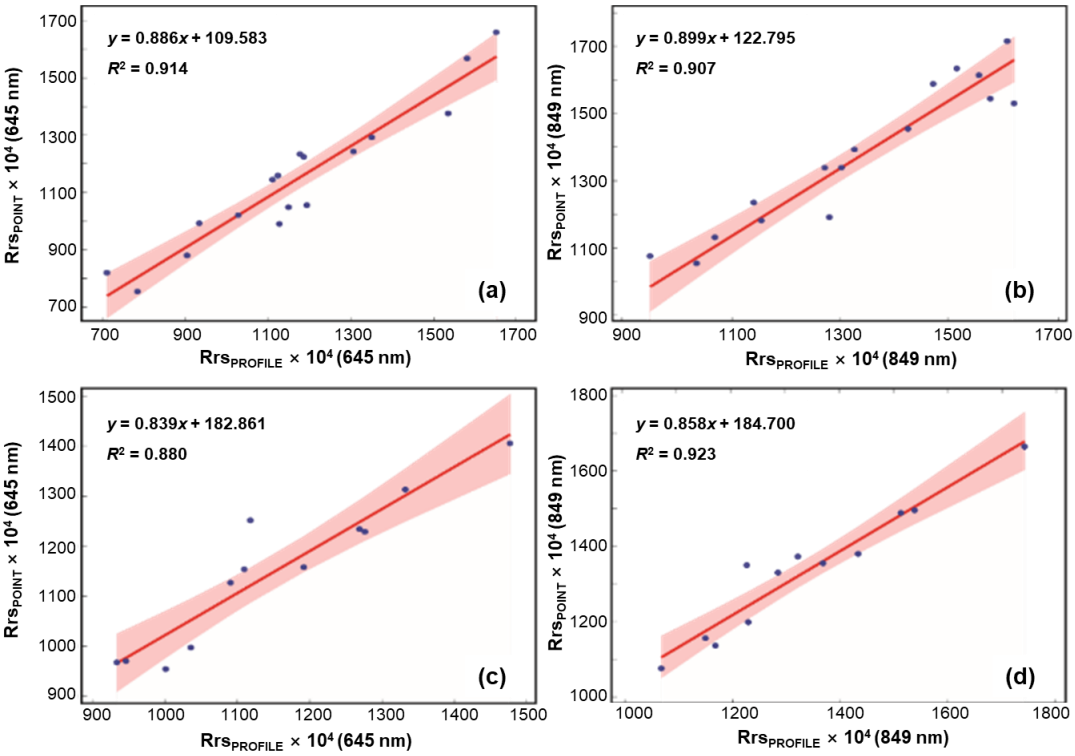


**Figure 7.** Correlation between the annual (a, b) and monthly (c, d) averages of the two data/pixel sampling methods (Profile = 39 pixels; Points = 37 pixels in each average).

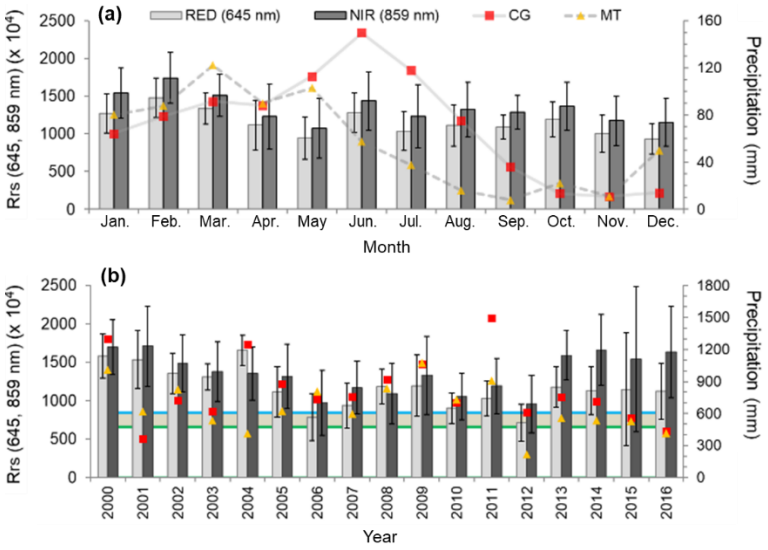


**Figure 8.** (a) Monthly and (b) annual averages of WSR filtered series for the $R_{RED}$ (645 nm) and $R_{NIR}$ (859 nm) bands and standard deviations, precipitation [at Campina Grande (CG) and Monteiro INMET (MT) stations], from 2000 to 2016.

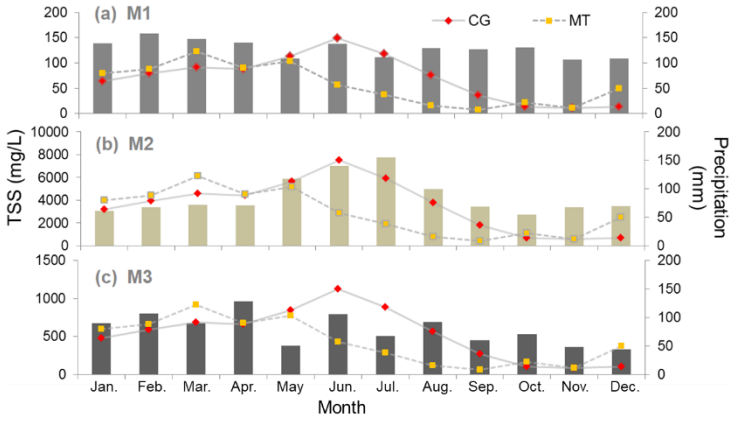


**Figure 9.** Monthly TSS estimates based on the (a) M1, (b) M2, and (c) M3 models and mean precipitation for CG and MT stations from 2000 to 2016.

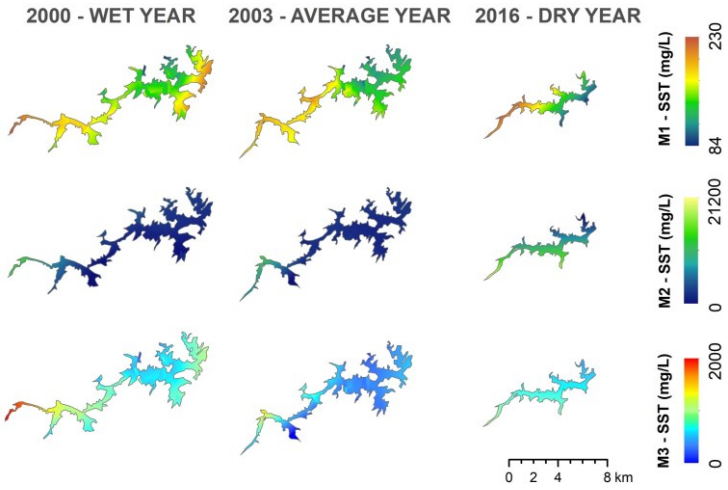


**Figure 10.** Interpolation of TSS using universal kriging for three precipitation conditions (wet, medium, and dry) at the Epitácio Pessoa Reservoir in 2000, 2003, and 2016, using M1, M2, and M3 models.

as a result, affect the spectral response of its sediment surface reflectance. Moreover, the last four years (Figure 8b) showed the highest WSR values of the $R_{NIR}$ band, as well as the largest deviations from the corresponding WSR values of the $R_{RED}$ band and the average pixel values, with more significant standard deviations observed in 2015. These indicators reaffirm the influence of prolonged droughts, with reductions in water volume and potential resuspension of sediments, reflected in the increase of WSR.

### 3.3. TSS Estimation

Figure 9 displays monthly TSS estimates based on the three models (M1, M2, and M3) and mean precipitation from 2000 ~ 2016. Due to the unavailability of observed monthly TSS data in the reservoir, the analysis was based on the rainfall patterns within the basin. The M1 model showed average TSS values of 128.8 ± 16.96 mg/L. Its monthly behavior mirrored the average data discussed for WSR values, possibly because the model is a linear regression.

The M2 model produced highly variable and disparate values for solids in water, with figures reaching nearly 8,000 mg/L in July and an average of 4,346.06 ± 1,665.53 mg/L, making it the model with the greatest fluctuation in monthly TSS averages. Despite the high TSS values, M2 showed a graphical pattern related to the precipitation values at the Campina Grande station (Figure 8a), with peaks in June, July, and August. Therefore, in an analysis of the monthly TSS average, M2 exhibited the graphical behavior that best matched one of the basin's weather conditions.

The M3 model estimated higher average TSS values during the first four months, followed by a decrease in May and an increase in June, aligning with the previously discussed average reflectance values. Unlike M1, its function is exponential, with a global average of 595.85 ± 201 mg/L and a maximum value in April (962.06 mg/L). In the annual analysis, the a priori model that most closely correlated with the observed field data was M3, showing a similar range in average TSS values: 270 to 961 mg/L for the estimates and 320 to 803 mg/L for the field data, with a linear correlation of 0.570. M1 was the model that presented the smallest TSS interval for annual averages, between 84 and 187 mg/L. The M2 model once again showed high TSS values, exceeding 20,000 mg/L in 2014. A possible explanation for the behavior of the monthly and annual M2 averages TSS might be the relationship between the $R_{NIR}/R_{RED}$ bands.

This spectral performance suggests the effect of physical, chemical, and biological differences in the sediment of the Brazilian semiarid region compared to the sediments produced in the Amazon basin, which experiences different climates and biomes, including the Caatinga biome. To represent different rainfall conditions, three years of the estimated TSS time series were selected based on Figure 8b (blue and green lines) and Santos et al. (2018): (a) rainy: a year with above-average rainfall, (b) average: a year with near-average rainfall, and (c) drought: a year with below-average rainfall), as shown in Figure 10.

For M1, the estimated TSS spatial distribution was similar in the three conditions. For the dry year, the contrast was more pronounced, while the rainy year also showed a higher TSS concentration near the dam wall. The M2 interpolation indicated lower TSS values across most reservoir surfaces during wet conditions (the year 2000) and average rainfall (the year 2003), around 2,350 mg/L, whereas the maximum values were observed during the dry condition.

It is noteworthy that the interpolation for M2 was not satisfactory as it estimated high negative values of TSS, which are physically inconsistent with the estimated variable. Therefore, the interval in Figure 10 was defined as 0 mg/L. The interpolation of M3 showed lower TSS concentrations in almost all the water bodies, except at the reservoir entrance. In the analysis of water surface reflectance and TSS variables, it is therefore possible to infer that both the conditions in a rainy year and during a dry period (prolonged drought) may influence the increase in TSS. In the first case, this is presumably related to the leaching and sediment input process, while in the second, it could be due to the reduction in water depth and volume, favoring the resuspension and higher concentration of sediments that are contained by the dam, thus affecting the sediment flow. Tables 1 and 2 show descriptive statistics of the variability of annual and monthly TSS estimates based on M1, M2, and M3 models. The results reveal that M1 had the lowest means, standard deviation, and mean deviation compared to the M2 and M3 models.

## 4. Discussion

### 4.1. Uncertainties and Difficulties of Water Surface Reflectance Data in the Reservoir

While previous studies have made efforts to utilize in situ remote sensing data and satellite data for water quality evaluation (Pal and Mohanty, 2002; Kumar et al., 2016; Yunus et al., 2021; Ashphaq et al., 2023), uncertainties and difficulties in acquiring water surface reflectance data in reservoirs present significant challenges. Various factors, including fluctuating water quality, the presence of aquatic vegetation, surface roughness, and atmospheric conditions, can impact data accuracy. These complications can undermine reliable monitoring and assessment of water quality, underscoring the need for robust techniques to mitigate these uncertainties. According to Balasubramanian et al. (2020), these uncertainties can stem from vegetation at the boundary or aquatic macrophytes, surface islands within the reservoir, bottlenecks in the channel, and clouds.

In this study, global mean WSR values ranged from 0.09 to 0.18, in line with other studies in semiarid regions (e.g., Pereira et al., 2019). Peak values in February and minimum values in May suggest the influence of rainfall over the reservoir drainage areas. Furthermore, our results showed high reflectance values for water ranging from 0 to 25% in the $R_{RED}$ band, which is consistent with values found in reservoirs in the Brazilian semiarid region (Mendonça et al., 2017), reservoirs of southeastern Brazil (Pinto et al., 2014; Condé et al., 2019), and lakes in the African semiarid region (Robert et al., 2017). These results reflect the data variability characteristic of the environmental conditions in the semiarid region, particularly the high spatiotemporal variability of precipitation and frequent droughts (Brito

**Table 1.** Descriptive Statistics Showing the Variability of Annual TSS Estimates (mg/L) Based on the Three Models Used

| Year | M1 | | | | | M2 | | | | | M3 | | | | |
|---|---|---|---|---|---|---|---|---|---|---|---|---|---|---|---|
| | M | SD | ME | Min | Max | M | SD | ME | Min | Max | M | SD | ME | Min | Max |
| 2000 | 176.9 | 33.7 | 25.3 | 107.2 | 269.2 | 2,462.0 | 2,871.3 | 1,864.7 | 455.1 | 12,149.9 | 828.5 | 619.7 | 476.4 | 8.6 | 2,828.8 |
| 2001 | 155.1 | 34.9 | 28.6 | 106.0 | 233.6 | 2,181.7 | 2,600.9 | 1,449.1 | 541.5 | 13,059.8 | 961.2 | 1,418.1 | 838.2 | 20.7 | 6,440.2 |
| 2002 | 145.5 | 34.8 | 25.9 | 89.5 | 256.1 | 2,591.7 | 3,051.7 | 2,025.6 | 253.8 | 13,952.9 | 581.8 | 693.5 | 454.1 | 25.4 | 3,013.6 |
| 2003 | 139.8 | 26.9 | 20.1 | 63.8 | 193.3 | 2,472.1 | 3,827.4 | 1,679.7 | 609.2 | 21,368.6 | 467.3 | 433.3 | 337.6 | 4.3 | 1,676.9 |
| 2004 | 187.2 | 25.5 | 18.4 | 124.3 | 252.4 | 931.6 | 687.6 | 514.7 | 206.1 | 3,202.6 | 399.2 | 236.9 | 200.7 | 36.1 | 912.1 |
| 2005 | 128.7 | 42.3 | 31.0 | 56.9 | 252.6 | 3,783.8 | 4,850.0 | 2,757.5 | 859.5 | 27,831.7 | 718.1 | 648.3 | 490.9 | 17.2 | 2,601.2 |
| 2006 | 84.0 | 34.9 | 26.3 | 37.7 | 189.3 | 3,437.3 | 2,572.0 | 2,004.2 | 673.1 | 12,328.4 | 267.9 | 313.9 | 241.2 | 2.3 | 1,268.0 |
| 2007 | 111.2 | 33.3 | 26.9 | 50.5 | 195.7 | 4,275.1 | 2,834.3 | 2,212.2 | 1,186.7 | 14,288.0 | 675.8 | 590.4 | 420.2 | 45.9 | 2,879.2 |
| 2008 | 137.7 | 26.3 | 21.6 | 93.0 | 183.8 | 1,617.3 | 1,163.5 | 771.7 | 485.5 | 5,956.8 | 399.8 | 421.9 | 323.9 | 8.9 | 1,628.2 |
| 2009 | 118.6 | 37.7 | 25.0 | 82.9 | 277.8 | 2,620.3 | 2,192.6 | 1,594.8 | 610.3 | 11,202.7 | 512.3 | 520.2 | 373.8 | 67.8 | 2,182.6 |
| 2010 | 98.5 | 30.1 | 22.5 | 14.9 | 149.3 | 3,457.8 | 3,425.0 | 2,142.1 | 738.7 | 18,278.1 | 491.4 | 418.0 | 339.0 | 0.0 | 1,414.7 |
| 2011 | 114.6 | 30.9 | 23.4 | 59.3 | 194.5 | 3,345.0 | 2,916.2 | 1,990.3 | 841.7 | 13,514.0 | 411.3 | 438.0 | 326.1 | 3.9 | 1,859.5 |
| 2012 | 91.7 | 46.5 | 27.1 | 24.2 | 309.7 | 5,107.5 | 4,108.8 | 2,768.0 | 1,351.3 | 18,780.4 | 526.1 | 902.7 | 487.2 | 0.6 | 4,286.1 |
| 2013 | 138.8 | 42.4 | 30.0 | 72.9 | 279.4 | 7,770.5 | 6,415.8 | 4,669.1 | 1,186.0 | 29,345.9 | 883.6 | 1,057.6 | 598.8 | 53.2 | 4,929.9 |
| 2014 | 111.1 | 35.3 | 28.2 | 45.0 | 177.3 | 17,185.0 | 17,870.9 | 1,0281.1 | 3,041.3 | 91,668.1 | 687.5 | 539.7 | 466.3 | 7.9 | 1,752.5 |
| 2015 | 117.7 | 22.9 | 17.9 | 74.7 | 162.4 | 8,175.1 | 5,112.3 | 3,856.9 | 3,647.7 | 20,352.4 | 952.5 | 1,273.8 | 898.1 | 103.8 | 4,297.0 |
| 2016 | 130.2 | 44.8 | 37.8 | 77.6 | 172.3 | 7,580.9 | 5,289.4 | 4,036.8 | 3,163.6 | 16,175.2 | 636.0 | 524.9 | 434.7 | 32.1 | 1,228.0 |

Note: M is average, SD is standard deviation, ME is mean deviation, Min is minimum, and Max is maximum.

**Table 2.** Descriptive Statistics Showing the Variability of Monthly TSS Estimates (mg/L) Based on the Three Models Used

| Month | M1 | | | | | M2 | | | | | M3 | | | | |
|---|---|---|---|---|---|---|---|---|---|---|---|---|---|---|---|
| | M | SD | ME | Min | Max | M | SD | ME | Min | Max | M | SD | ME | Min | Max |
| Jan. | 138.8 | 21.5 | 15.9 | 92.1 | 209.0 | 3,050.1 | 1,723.0 | 1,226.0 | 1,070.9 | 8,730.0 | 673.0 | 789.7 | 408.3 | 45.3 | 4,937.3 |
| Feb. | 158.4 | 26.9 | 20.8 | 93.8 | 226.5 | 3,386.2 | 2,097.4 | 1,503.4 | 1,055.1 | 11,964.9 | 803.6 | 782.5 | 521.8 | 32.6 | 4,074.7 |
| Mar. | 147.8 | 26.3 | 21.4 | 100.0 | 205.1 | 3,569.4 | 1,990.8 | 1,499.1 | 962.7 | 9,055.3 | 675.2 | 825.0 | 479.9 | 32.9 | 4,468.7 |
| Apr. | 140.8 | 51.8 | 33.2 | 34.5 | 321.4 | 3,530.8 | 3,656.5 | 2,296.5 | 1,006.2 | 20,237.5 | 962.1 | 1,600.0 | 942.5 | 0.4 | 7,942.1 |
| May | 108.7 | 28.6 | 21.3 | 48.5 | 186.0 | 5,901.6 | 5,066.1 | 3,766.7 | 623.1 | 20,388.2 | 377.1 | 400.9 | 298.6 | 2.7 | 1,792.9 |
| Jun. | 138.2 | 29.7 | 23.5 | 79.0 | 213.7 | 7,004.7 | 7,736.5 | 4,811.1 | 615.5 | 35,698.1 | 794.8 | 671.3 | 499.5 | 106.6 | 2,860.1 |
| Jul. | 111.8 | 22.2 | 19.1 | 68.5 | 153.5 | 7,753.6 | 6,143.5 | 4,359.5 | 677.0 | 28,485.7 | 502.4 | 537.9 | 368.2 | 1.9 | 2,820.5 |
| Aug. | 129.7 | 36.0 | 27.0 | 81.2 | 252.2 | 4,967.9 | 3,416.0 | 2,459.9 | 998.3 | 16,090.2 | 688.7 | 656.7 | 422.1 | 111.6 | 3,707.2 |
| Sep. | 126.6 | 22.6 | 17.6 | 84.3 | 189.5 | 3,414.8 | 2,412.6 | 1,647.8 | 1,099.6 | 13,660.9 | 453.5 | 307.8 | 249.4 | 8.7 | 1,367.6 |
| Oct. | 130.1 | 26.8 | 20.7 | 74.0 | 183.1 | 2,752.7 | 2,194.3 | 1,072.5 | 772.0 | 14,345.9 | 527.1 | 530.2 | 333.6 | 59.9 | 2,597.8 |
| Nov. | 106.8 | 28.7 | 20.1 | 55.4 | 194.4 | 3,368.2 | 2,682.0 | 1,624.7 | 542.6 | 15,955.2 | 363.8 | 447.8 | 295.0 | 0.3 | 2,311.3 |
| Dec. | 108.5 | 39.7 | 23.0 | 56.8 | 300.8 | 3,452.9 | 1,892.2 | 1,424.1 | 830.7 | 8,548.2 | 328.9 | 272.6 | 225.3 | 7.6 | 946.4 |

Note: M is average, SD is standard deviation, ME is mean deviation, Min is minimum, and Max is maximum.

et al., 2021; Neto et al., 2021).

Assessing water bodies, especially reservoirs, brings unique challenges due to their volumetric and topographic conditions. These challenges arise not from the methodology proposed in this study but rather from the reservoir's inherent volumetric and topographic characteristics. These conditions preclude a continuous analysis of WSR behavior between the reservoir inlet and outlet. Studies by Pinto et al. (2014) and Condé et al. (2019) report a higher sediment input (i.e., reflectance) at the reservoir entrance compared to the area near the dam wall, a result of the hydrodynamic transition from lotic to lentic environments.

The monthly and annual averages of the filtered water surface reflectance (WSR) series for the $R_{RED}$ and $R_{NIR}$ bands revealed certain patterns. The highest monthly reflectance averages in the WSR series are observed from January to March, as well as in June for the $R_{NIR}$ band. For the $R_{RED}$ band, there is a slight reduction in reflectance values, particularly in December. These patterns suggest that the reservoir responds to rainfall patterns in Paraíba State, as supported by Santos et al. (2018, 2019) and Neto et al. (2021). These authors analyzed TRMM data for Cariri Paraibano from 1998 to 2015, specifically noting the maximum monthly averages in March and minima in recent months.

Moreover, a potential cause of the high WSR response in the $R_{NIR}$ band could be the presence of suspended algae due to the prolonged drought period in the semiarid area (Braga et al., 2015), especially in 2016. However, this effect might not be as impactful. For instance, Cavalcante et al. (2017) reported chlorophyll-a (Chla) values below 10 μg/L in 2016, with low values in September, August, and October. Furthermore, Dogliotti et al. (2015) emphasize that chlorophyll-a only significantly interferes with the spectral response when its concentration exceeds 30 μg/L.

### 4.2. Spatiotemporal Variability of TSS

The main goal behind developing and fine-tuning a robust TSS model was to evaluate the estimated sediment in the reservoir. The estimated results indicate high variations in the simulated TSS values due to precipitation variability in the region. Villar et al. (2013), while identifying the optimal band for generating the TSS model, concluded that there was a seasonal dependence, likely due to changes in the sediment's particle size distribution over the annual cycle, most notably during the flood period. Simultaneously, these authors demonstrated graphically that the values of the $R_{RED}$ band were consistently higher than those of the $R_{NIR}$ band. However, in this study, the behavior was the opposite; almost always, the highest averages came from the $R_{NIR}$ band.

Mohanty and Pal (2001) attempted to predict TSS concentration using LISS-I (IRS-IB) data and incorporated the Soil Brightness Index (SBI). However, the coefficients used in their algorithm were obtained from existing literature. It is important to note that IRS data has limited sensitivity and temporal frequency compared to MODIS data, which might impact the accuracy and reliability of the TSS concentration mapping. MODIS data offer numerous advantages over this specific product, including high temporal resolution, high sensitivity with a 12-bit radiometric resolution, cost-effectiveness, and, notably, exemption from the complexities associated with atmospheric correction (Kumar et al., 2016). Likewise, Robert et al. (2017) reported changes in sediment concentration in the Gourma region (Africa), suggesting wind resuspension during the drought period. Although this phenomenon does not significantly influence the sediments of the Epitácio Pessoa Reservoir, as in the case of Robert et al. (2017), the river regime in the Cariri region is torrential and temporary, marked by violent floods, rapid recession, zero discharge for most of the dry season, and years with no runoff. The dry season is characterized by a gradual lowering of river levels until they dry out, punctuated by abrupt floods (Nascimento and Alves, 2008).

These values align closely with those obtained by Coelho et al. (2017), who, while monitoring reservoirs in Ceará (located in the Brazilian semiarid region), found TSS values ranging between 2.3 ~ 129 mg/L during the rainy season in the Paus Brancos Reservoir. However, these values are discordant with those reported by Molisani et al. (2013), who found values ranging from 0.72 to 25 mg/L in reservoirs in the same state. Meanwhile, six-monthly observed data from the State Environment Agency of Paraíba (SUDEMA) at the analyzed reservoir ranged from 288 ~ 1,094 mg/L. Thus, it is evident that even though they are reservoirs in a semiarid region, these reservoirs can exhibit vastly different values.

### 4.3. Challenges and Application

This study underscores the vital importance of estimating TSS in reservoirs, a task that has often been challenging due to insufficient monitoring, particularly in regions with intermittent waterways. The present research employs remote sensing products and geotechnological techniques for estimating WSR and TSS in the Epitácio Pessoa Reservoir, addressing a significant gap in our understanding of reservoir sediments. Practical applications of these estimates range from assessing the presence of heavy metals in sediments to prevent health risks, to monitoring water pollution, identifying erosion processes, and estimating reservoir siltation. Comparatively, other studies have used similar methods to estimate TSS in various environments, but estimates have been scarce in reservoirs in the Brazilian semiarid region due to its unique climatic, floristic, and geological characteristics.

The geological characteristic of the watershed is one of the key factors influencing TSS. Given its primarily crystalline bedrock composition, the study area lacks groundwater storage, contributing to increased flow after intense rainfall events and leading to the rapid transport of solid materials to rivers. In the Brazilian semiarid region, it has been found that sediment transport is often strongly disconnected, with high sediment loads transported during extreme rainfall events. Estimating WSR and TSS using MODIS images for reservoirs like Epitácio Pessoa can lead to effective measures to protect and preserve water resources. However, understanding the limitations of these techniques is essential. Sources of uncertainty include the presence of clouds, aerosols, nearby vegetation, and the need for calibration and validation of collected data.

However, the present study has demonstrated a strong correlation between the annual and monthly averages extracted by different sampled pixels, providing evidence for the efficacy of this approach. Compared to the work of Zhang et al. (2014), which used a radiative transfer model to estimate TSS, this study leverages the temporal monitoring capabilities of MODIS images. Ultimately, the results of this study contribute significantly to understanding sediment transport and its implications for water policy in semiarid regions. It provides a novel, validated approach for TSS and WSR estimation using MODIS images, paving the way for improved water resources management in areas where surface reservoirs are the primary water supply.

## 5. Conclusions

The study estimated the spatiotemporal dynamics of WSR and TSS in the Epitácio Pessoa Reservoir from 2000 to 2016 using automated methods and MODIS images. Quantitative results reveal a strong correlation ($R > 0.93$) between the annual and monthly averages extracted by different and independent sampled pixels. The proposed methodology demonstrated satisfactory performance, particularly when removing pixels with total or partial cloud presence or solid indications of spectral mixing, which was achieved through different vectorized masks.

The use of MODIS data in the Brazilian semiarid region proved beneficial, primarily due to its high temporal data frequency. However, its low spatial resolution presents a limitation. The results revealed that this data has specific constraints for the region. These issues must be carefully analyzed for each object under study and research objective, such as the Epitácio Pessoa Reservoir, which has a wide interannual variability of its water mirror, varying nearly seven times its size throughout the study period.

The methodology was found to capture the reflectance variability in periods of contrast (dry and rainy) within the region effectively. The near-infrared band reflectance values were typically higher than the red band, except in 2004 and 2008, when changes in the sediment type were observed due to the sudden increase in reservoir volume. This reveals the methodology's ability to reflect significant environmental changes in the reservoir.

However, the limitations of this study include its dependence on a single reservoir for testing the models, a variable that may affect the generalizability of the results. The study also primarily utilized MODIS images, and while this has proven effective, future research could benefit from the inclusion of different data sources to provide more comprehensive results. The spatial resolution of the MODIS data also presents a potential limit to the precision of the results.

The results of this study could prove useful for public policies managing water resources in the region, including the integrated water management plan of the Epitácio Pessoa Reservoir. Furthermore, the results could be used in future studies estimating silting and the amount of sediment yield in the basin and its arrival in the reservoir.

Given the successful application of the methodology, it is recommended for future research to consider testing new multispectral image data, such as Sentinel-2, which has a spatial resolution of 10 m, for assessing TSS and WSR. Further, the results of this study might be applied to forecast silting, sediment yield, and water quality in reservoirs within semiarid regions using MODIS images.

**Acknowledgments.** This study was financed in part by the Brazilian Federal Agency for the Support and Evaluation of Graduate (Coordenação de Aperfeiçoamento de Pessoal de Nível Superior - CAPES) – Fund Code 001, National Council for Scientific and Technological Development, Brazil – CNPq (Grant No. 313358/2021-4, 309330/2021-1, and 420031/2021-9) and Federal University of Paraíba.

## References

AESA. State water management executive agency of Paraíba. Monitoramento: Açudes. João Pessoa (PB). http://www.aesa.pb.gov.br/aesa/volumesAcudes.do?metodo=listarAcudesUltimaCota/(accessed October 15, 2016).

AESA. State Water management executive agency of Paraíba. Monitoramento: Climatologia. João Pessoa (PB). http://site2.aesa.pb.gov.br/aesa/jsp/monitoramento/chuvas/climatologiasGraficos.jsp/ (accessed February 15, 2018).

ANA (2013). *National Water and Sanitation Agency of Brazil*. Technical Note nº. 068/2013/ SGI-ANA. Elevation × Area × Volume Curves of the Epitácio Pessoa-Boqueirão Dam, PB.

Ashphaq, M., Srivastava, P.K., Mitra, D. (2023). Preliminary examination of influence of chlorophyll, total suspended material, and turbidity on satellite derived-bathymetry estimation in coastal turbid water. *Reg. Stud. Mar. Sci*., 62, 102920. https://doi.org/10.1016/j.rsma.2023.102920

Assis, K.G.O., da Silva, Y.J.A.B., Lopes, J.W.B., Medeiros, J.C., Teixeira, M.P.R., Rimá, F.B. and Singh, V.P. (2021). Soil loss and sediment yield in a perennial catchment in southwest Piauí, Brazil. *Environ. Monit. Assess.,* 193, 26. https://doi.org/10.1007/s10661-020-08789-y

Balasubramanian, S.V., Pahlevan, N., Smith, B., Binding, C., Schalles, J., Loisel, H., Gurlin, D., Greb, S., Alikas, K., Randla, M., Bunkei, M., Moses, W., Nguyễn, H., Lehmann, M.K., O'Donnell, D., Ondrusek, M., Han, T.H., Fichot, C.G., Moore, T. and Boss, E. (2020). Robust algorithm for estimating total suspended solids (TSS) in inland and nearshore coastal waters. *Remote Sens. Environ.*, 246, 111768. https://doi.org/10.1016/j.rse.2020.111768

Becker, R.H., Sultan, M.I., Boyer, G.L., Twiss, M.R. and Konopko, E. (2009). Mapping cyanobacterial blooms in the great lakes using MODIS. *J. Great Lakes Res.*, 35(3), 447-453. https://doi.org/10.1016/j.jglr.2009.05.007

Bernardo, N., Watanabe, F., Rodrigues, T. and Alcantâra, E. (2016). Evaluation of the suitability of MODIS, OLCI and OLI for mapping the distribution of total suspended matter in the Barra Bonita Reservoir (Tietê River, Brazil). *Remote Sens. Appl.*, 4, 68-82. https://doi.org/10.1016/j.rsase.2016.06.002

Braga, G.G., Becker, V., Oliveira, J.N.P., Mendonça Jr, J.R., Bezerra, A.F.M., Torres, L.M., Galvão, A.M.F. and Mattos, A. (2015). Influence of extended drought on water quality in tropical reservoirs in a semiarid region. *Acta Limnol. Bras.*, 27(1), 15-23. https://doi.org/10.1590/S2179-975X2214

Brasil Neto, R.M., Santos, C.A.G., da Silva, R.M., dos Santos, C.A.C., Liu, Z. and Quinn, N.W. (2021). Geospatial cluster analysis of the state, duration and severity of drought over Paraíba State, northeastern Brazil. *Sci. Total. Environ.*, 799, 149492. https://doi.org/10.1016/j.scitotenv.2021.149492

Brasil Neto, R.M., Santos, C.A.G., Silva, R.M. and Santos, C.A.C. (2022). Evaluation of TRMM satellite dataset for monitoring meteorological drought in northeastern Brazil. *Hydrolog. Sci. J.*, 67(14), 2100-2120. https://doi.org/10.1080/02626667.2022.2130333

Brito, C.S., da Silva, R.M., Santos, C.A.G., Brasil Neto, R.M. and Coelho, V.H.R. (2021). Monitoring meteorological drought in a semiarid region using two long-term satellite-estimated rainfall datasets: A case study of the Piranhas River basin, northeastern Brazil. *Atmos. Res*., 250, 105380. https://doi.org/10.1016/j.atmosres.2020.105380

Brown, C.A., Huot, Y., Werdell, P.J., Gentili, B. and Claustre, H. (2008). The origin and global distribution of second order variability in satellite ocean color and its potential applications to algorithm development. *Remote Sens. Environ.*, 112(12), 4186-4203. https://doi.org/10.1016/j.rse.2008.06.008

Cavalcante, H., Cruz, P., Viana, L., Silva, D. and Barbosa, J. (2017). Influence of the use and the land cover of the catchment in the water quality of the semiarid tropical reservoirs. *J. Remote Sens. Technol.*, 7(7), 389-398. https://doi.org/10.29150/jhrs.v7.7.p389-398

Coelho, C., Heim, B., Foerster, S., Brosinsky, A. and De Araújo, J.C. (2017). In situ and satellite observation of CDOM and chlorophyll-a dynamics in small water surface reservoirs in the Brazilian semiarid region. *Water*, 9(12), 913-935. https://doi.org/10.3390/w9120913

Condé, R.C., Martinez, J.M., Pessotto, M.A., Villar, R., Cochonneau, G., Henry, R., Lopes, W. and Nogueira, M. (2019). Indirect assessment of sedimentation in hydropower dams using MODIS remote sensing images. *Remote Sens.*, 11(3), 314-335. https://doi.org/10.3390/rs11030314

Da Silva, R.M., Silva, J.F.C.B.C., Santos, C.A.G., Silva, A.M. and Brasil Neto, R.M. (2020). Spatial distribution and estimation of rainfall trends and erosivity in the Epitácio Pessoa reservoir catchment, Paraíba - Brazil. *Nat. Hazards*, 102, 829-849. https://doi.org/10.1007/s11069-020-03926-9

Dantas, J.C., Silva, R.M. and Santos, C.A.G. (2020). Drought impacts, social organization and public policies in northeastern Brazil: A case study of the Upper Paraíba River basin. *Environ. Monit Assess*., 192, 317. https://doi.org/10.1007/s10661-020-8219-0

De Lira Azevêdo, E., de Lucena Barbosa, J.E., Viana, L.G., Anacleto, M.J.P., Callisto, M. and Molozzi, J. (2017). Application of a statistical model for the assessment of environmental quality in neotropi-

cal semi-arid reservoirs. *Environ. Monit. Assess*., 189, 65. https://doi.org/10.1007/s10661-016-5723-3

De Medeiros, I.C., Da Costa Silva, J.F.C.B., Silva, R.M. and Santos, C.A.G. (2019). Run-off-erosion modelling and water balance in the Epitácio Pessoa Dam river basin, Paraíba State in Brazil. *Int. J. Environ. Sci. Technol.*, 16(7), 3035-3048, 545-562. https://doi.org/10.1007/s13762-018-1940-3

De Mendonça, J., Lopes, F., Andrade, E., Oliveira Lima, F. and Da Silva, F. (2017). Monitoring water quality in a reservoir of the semi-arid region using remote sensing. *J. Exp. Agric. Int.*, 19(1), 1-12. https://doi.org/10.9734/JEAI/2017/37913

De Sousa, M.C., Veloso, G.V., Gomes, L.C., Fernandes-Filho, E.I. and de Oliveira, T.S. (2021). Spatio-temporal dynamics of land use changes of an intense anthropized basin in the Brazilian semi-arid region. *Remote Sens. Appl.*, 24, 100646. https://doi.org/10.1016/j.rsase.2021.100646

Dogliotti, A.I., Ruddick, K.G., Nechad, B., Doxaran, D. and Knaeps, E. (2015). A single algorithm to retrieve turbidity from remotely-sensed data in all coastal and estuarine waters. *Remote Sens. Environ.*, 156, 157-168. https://doi.org/10.1016/j.rse.2014.09.020

Dorji, P., Fearns, P. and Broomhall, M. (2016). A semi-analytic model for estimating total suspended sediment concentration in turbid coastal waters of northern Western Australia using MODIS-Aqua 250 m data. *Remote Sens*., 8(7), 556. https://doi.org/10.3390/rs8070556

Doxaran, D., Froidefond, J.-M., Lavender, S. and Castaing, P. (2002). Spectral signature of highly turbid waters: Application with SPOT data to quantify suspended particulate matter concentrations. *Remote Sens. Environ.*, 81(1), 149-161. https://doi.org/10.1016/S0034-4257(01)00341-8

Fettweis, M., Riethmüller, R., Verney, R., Becker, M., Backers, J., Baeye, M., Chapalain, M., Claeys, S., Claus, J., Cox, T., Deloffre, J., Depreiter, D., Druine, F., Flöser, G., Grünler, S., Jourdin, F., Lafite, R., Nauw, J., Nechad, B., Röttgers, R., Sottolichio, A., Van Engeland, T., Vanhaverbeke, W. and Vereecken, H. (2019). Uncertainties associated with in situ high-frequency long-term observations of suspended particulate matter concentration using optical and acoustic sensors. *Prog. Oceanogr*., 178, 102162. https://doi.org/10.1016/j.pocean.2019.102162

Fonseca, C.A.B., Al-Ansari, N., Silva, R.M., Santos, C.A.G., Zerouali, B., Oliveira, D.B. and Elbeltagi, A. (2022). Investigating relationships between runoff-erosion processes and land use and land cover using remote sensing multiple gridded datasets. *ISPRS Int. J. Geoinf.*, 11, 272. https://doi.org/10.3390/ijgi11050272

Fuentes, I., Scalzo, R. and Vervoort, R.W. (2021). Volume and uncertainty estimates of on-farm reservoirs using surface reflec-tance and LiDAR data. *Environ. Model. Softw.*, 143, 105095 https://doi.org/10.1016/j.envsoft.2021.105095

Han, Z., Jin, Y.Q. and Yun, C.X. (2006). Suspended sediment concentrations in the Yangtze River estuary retrieved from the CMODIS data. *Int. J. Remote Sens.*, 27 (19), 4329-4336. https://doi.org/10.1080/01431160600658164

Hooke, J. and Souza, J.O.P. (2021). Challenges of mapping, modelling and quantifying sediment connectivity. *Earth-Sci. Rev*., 223, 103847. https://doi.org/10.1016/j.earscirev.2021.103847

Isidro, C.M., McIntyre, N., Lechner, A.M. and Callow, I. (2018). Quantifying suspended solids in small rivers using satellite data. *Sci. Total Environ.*, 634, 1554-1562. https://doi.org/10.1016/j.scitotenv.2018.04.006

Jiang, D., Matsushita, B., Pahlevan, N., Gurlin, D., Lehmann, M.K., Fichot, C.G., Schalles, J., Loisel, H., Binding, C., Zhang, Y., Alikas, K., Kangro, K., Uusõue, M., Ondrusek, M., Greb, S., Moses, W.J., Lohrenz, S. and O'Donnell, D. (2021). Remotely estimating total suspended solids concentration in clear to extremely turbid waters using a novel semi-analytical method. *Remote Sens. of Environ.*, 258, 112386. https://doi.org/10.1016/j.rse.2021.112386

Kim, H.C., Son, S., Kim, Y.H., Khim, J.S., Nam, J., Chang, W.K., Lee, J.H., Lee, C.H. and Ryu, J. (2017). Remote sensing and water quality indicators in the Korean West coast: Spatio-temporal structures of MODIS-derived chlorophyll-a and total suspended solids. *Mar. Pollut. Bull*., 121(1-2), 425-434. https://doi.org/10.1016/j.marpolbul.2017.05.026

Kumar, A., Equeenuddin, S.M., Mishra, D.R. and Acharya, B.C. (2016). Remote monitoring of sediment dynamics in a coastal lagoon: Long-term spatio-temporal variability of suspended sediment in Chilika. *Estuar. Coast. Shelf S*., 170, 155-172. https://doi.org/10.1016/j.ecss.2016.01.018

Lima Neto, I.E., Medeiros, P.H.A., Costa, A.C., Wiegand, M.C., Barros, A.R.M. and Barros, M.U.G. (2022). Assessment of phosphorus loading dynamics in a tropical reservoir with high seasonal water level changes. *Sci. Total Environ.*, 815, 152875. https://doi.org/10.1016/j.scitotenv.2021.152875

Luo, W., Shen, F., He, Q., Cao, F., Zhao, H. and Li, M. (2022). Changes in suspended sediments in the Yangtze River Estuary from 1984 to 2020: Responses to basin and estuarine engineering con-structions. *Sci. Total Environ.*, 805, 150381. https://doi.org/10.1016/j.scitotenv.2021.150381

Manoppo, K. and Budhiman, S. (2017). Estimation on the concentration of total suspended matter in Lombok Coastal using Landsat 8 OLI, Indonesia. *IOP Conference Series: Environ. Earth Sci*., IOP Publishing

Mao, Z., Chen, J., Pan, D., Tao, B. and Zhu, Q. (2012). A regional remote sensing algorithm for total suspended matter in the East China Sea. *Remote Sens. Environ.*, 124, 819-831. https://doi.org/10.1016/j.rse.2012.06.014

Miller, R.L. and Mckee, B.A. (2004). Using MODIS Terra 250 m imagery to map concentrations of total suspended matter in coastal waters. *Remote Sens. Environ.*, 93(1-2), 259-266. https://doi.org/10.1016/j.rse.2004.07.012

Mishra, D.R. and Mishra, S. (2010). Plume and bloom: Effect of Mississippi river diversion on the water quality of Lake Pontchar-train, *Geocarto Int.*, 25(7), 555-568. https://doi.org/10.1080/10106041003763394

Molisani, M.M., Becker, H., Barroso, H.S., Hijo, C.A.G., Monte, T.M., Vasconcellos, G.H. and Lacerda, L.D. (2013). The influence of Castanhão reservoir on nutrient and suspended matter transport during rainy season in the ephemeral Jaguaribe river (CE, Brazil). *Braz. J. Biol.*, 73(1), 115-123. https://doi.org/10.1590/S1519-69842013000100013

Nechad, B., Ruddick, K.G. and Park, Y. (2010). Calibration and validation of a generic multisensor algorithm for mapping of total suspended matter in turbid waters. *Remote Sens. Environ.*, 114(4), 854-866. https://doi.org/10.1016/j.rse.2009.11.022

Pahlevan, N. and Schott, J.R. (2012). Characterizing the relative calibration of Landsat-7 (ETM+) visible bands with Terra (MODIS) over clear waters: The implications for monitoring water resources. *Remote Sens. Environ.*, 125, 167-180. https://doi.org/10.1016/j.rse.2012.07.013

Pal, S.R., and P.K. Mohanty, 2002. Use of IRS-1B data for change detection in water quality and vegetation of Chilika Lagoon, east coast of India. *Int. J. Remote Sens.*, 23(6), 1027-1042. https://doi.org/10.1080/01431160110076243

Pereira, F.J.S., Costa, C.A.G., Foerster, S., Brosinsk, A. and Araújo, J.C. (2019). Estimation of suspended sediment concentration in an intermittent river using multi-temporal high-resolution satellite imagery. *Int. J. Appl. Earth. Obs. Geoinf.*, 79, 153-161. https://doi.org/10.1016/j.jag.2019.02.009

Pinto, C.E.T., Menezes, P.H.B.J., Martinez, J., Roig, H.L. and Villar, R.A.E. (2014). Use of MODIS images to monitor the sediment inflow into the Três Marias reservoir. *Rev. Bras. Eng. Agric. Ambient.*, 18(5), 507-516. https://doi.org/10.1590/S1415-43662014000500007

Robert, E., Grippa, M., Kergoat, L., Pinet, S., Gal, L., Cochonneau, G. and Martinez, J. (2016). Monitoring water turbidity and surface sus-

pended sediment concentration of the Bagre Reservoir (Burkina Faso) using MODIS and field reflectance data. *Int. J. Appl. Earth. Obs. Geoinf.*, 52, 243-251. https://doi.org/10.1016/j.jag.2016.06.016

Robert, E., Kergoat, L., Soumaguel, N., Merlet, S., Martinez, J.M., Diawara, M. and Grippa, M. (2017). Analysis of suspended particulate matter and its drivers in Sahelian Ponds and Lakes by remote sensing (Landsat and MODIS): Gourma Region, Mali. *Remote Sens.*, 9(12), 1272. https://doi.org/10.3390/rs9121272

Sahoo, D.P., Sahoo, B. and Tiwari, M.K. (2022). MODIS-Landsat fusion-based single-band algorithms for TSS and turbidity estimation in an urban-waste-dominated river reach. *Water Res.*, 224, 119082. https://doi.org/10.1016/j.watres.2022.119082

Santos do Nascimento, S. and Alves, J.J.A. (2008). Ecoclimatology of the Cariri Paraibano. *Rev. Geogr. Acad.*, 2(3), 28-41.

Santos, C.A.G., Brasil Neto, R.M., da Silva, R.M. and Costa, S.G.F. (2019). Cluster analysis applied to spatiotemporal variability of monthly precipitation over Paraíba State using Tropical Rainfall Measuring Mission (TRMM) Data. *Remote Sens.*, 11(6), 637. https://doi.org/10.3390/rs11060637

Santos, C.A.G., Brasil Neto, R.M., da Silva, R.M. and Santos, D.C. (2018). Innovative approach for geospatial drought severity classification: A case study of Paraíba state, Brazil. *Stoch. Environ. Res. Risk Assess.*, 33(2), 545-562. https://doi.org/10.1007/s00477-018-1619-9

Santos, J.Y.G., Montenegro, S.M.G.L., Silva, R.M., Santos, C.A.G., Quinn, N.W., Xavier, A.P.C. and Ribeiro Neto, A. (2021). Modeling the impacts of future LULC and climate change on runoff and sediment yield in a strategic basin in the Caatinga/Atlantic forest ecotone of Brazil. *Catena*, 203, 105308. https://doi.org/ 10.1016/j.catena.2021.105308

Silva, A.M., Silva, R.M. and Santos, C.A.G. (2019). Automated surface energy balance algorithm for land (ASEBAL) based on automating endmember pixel selection for evapotranspiration calculation in MODIS orbital images. *Int. J. Appl. Earth. Obs. Geoinf.*, 79, 1-11. https://doi.org/10.1016/j.jag.2019.02.012

Silva, A.M., Silva, R.M., Santos, C.A.G., Linhares, F.M. and Xavier, A.P.C. (2022). Modeling the effects of future climate and land use changes on streamflow in a headwater basin in the Brazilian Caatinga biome. *Geocarto Int.*, 37, 12436-12465. https://doi.org/10.1080/10106049.2022.2068672

Silva, J.F.C.B.C., da Silva, R.M., Santos, C.A.G., Silva, A.M. and Vianna, P.C.G. (2021). Analysis of the response of the Epitácio Pessoa reservoir (Brazilian semiarid region) to potential future drought, water transfer and LULC scenarios. *Nat. Hazards*, 108, 1347-1371. https://doi.org/10.1007/s11069-021-04736-3

Silva, R.M., Santos, C.A.G. and Dos Santos, J.Y.G. (2018). Evaluation and modeling of runoff and sediment yield for different land covers under simulated rain in a semiarid region of Brazil. *Int. J. Sediment Res.*, 33(2), 117-125. https://doi.org/10.1016/j.ijsrc.2017.04.005

Souza, J.O.P. and Hooke, J. (2021). Influence of seasonal vegetation dynamics on hydrological connectivity in tropical drylands. *Hydrol. Process.*, 35, 1-19. https://doi.org/10.1002/hyp.14427

Tassan, S. (1993). An improved in-water algorithm for the determination of chlorophyll and suspended sediment concentration from Thematic Mapper data in coastal waters. *Int. J. Remote Sens.*, 14(6), 1221-1229. https://doi.org/10.1080/01431169308904406

Vermote, E.F. (2015). *MOD09Q1 MODIS/Terra Surface Reflectance 8-Day L3 Global 250m SIN Grid V006.* Distributed by NASA EOSDIS LP DAAC. https://doi.org/10.5067/MODIS/MOD09Q1.006

Vermote, E.F., Tanre, D., Deuze, J.L., Herman, M.A. and Morcette, J.J.A. (1997). Second simulation of the satellite signal in the solar spectrum, 6S: An overview. *IEEE Trans. Geosci. Remote Sens.*, 35(3), 675-686. https://doi.org/10.1109/36.581987

Viana, J.F.S., Montenegro, S.M.G.L., Silva, B.B., Silva. R.M., Srinivasan, R., Santos, C.A.G., Araujo, D.C.S. and Tavares, C.G. (2021). Evaluation of gridded meteorological datasets and their potential hydrological application to a humid area with scarce data for Pirapama River basin, northeastern Brazil. *Theor. Appl. Climatol.*, 145, 393-410. https://doi.org/10.1007/s00704-021-03628-7

Villar, R.E., Martinez, J.M., Le Texier, M., Guyot, J.L., Fraizy, P. and Meneses, P.R. (2013). A study of sediment transport in the Madeira River, Brazil, using MODIS remote-sensing images. *J. S. Am. Earth Sci.*, 44(1), 45-54. https://doi.org/10.1016/j.jsames.2012.11.006

Wan, Z., and Li, Z. L. (1997). A physics-based algorithm for retrieving land-surface emissivity and temperature from EOS/MODIS data. *IEEE Trans. Geosci. Remote Sens.*, 35(4), 980-996. https://doi.org/10.1109/36.602541

Watanabe, F.S.Y., Alcântara, E., Rodrigues, T.W.P., Imai, N.N., Barbosa, C.C.F. and Rotta, L.H.S. (2015). Estimation of chlorophyll-a concentration and the trophic state of the Barra Bonita hydroelectric reservoir using OLI/Landsat-8 images. *Int. J. Environ.*, 12(9), 10391-10417. https://doi.org/10.3390/ijerph120910391

Yunus, A.P., Masago, Y. and Hijioka, Y. (2021). Analysis of long-term (2002–2020) trends and peak events in total suspended solids concentrations in the Chesapeake Bay using MODIS imagery. *J. Environ.*, 299, 113550. https://doi.org/10.1016/j.jenvman.2021.113550

Zhang, M., Dong, Q., Cui, T., Xue, C. and Zhang, S. (2014). Suspended sediment monitoring and assessment for Yellow River estuary from Landsat TM and ETM+ imagery. *Remote Sens. Environ.*, 146, 136-147. https://doi.org/10.1016/j.rse.2013.09.033

Zhang, M., Tang, J., Dong, Q., Song, Q. and Ding, J. (2010). Retrieval of total suspended matter concentration in the Yellow and East China Seas from MODIS imagery. *Remote Sens. Environ.*, 114(2), 392-403. https://doi.org/10.1016/j.rse.2009.09.016

Zhang, S., Foerster, S., Medeiros, P., de Araújo, J.C., Motagh, M. and Waske, B. (2016). Bathymetric survey of water reservoirs in northeastern Brazil based on TanDEM-X satellite data. *Sci. Total Environ.*, 571, 575-593. https://doi.org/10.1016/j.scitotenv.2016.07.02